

Supporting Information for:  
Lipid exchange enhances geometric pinning  
in multicomponent membranes on patterned substrates

Melissa Rinaldin<sup>1,2</sup>, Piermarco Fonda<sup>1</sup>, Luca Giomi<sup>1</sup>, and Daniela J. Kraft<sup>2</sup>

<sup>1</sup>Instituut-Lorentz, Universiteit Leiden, P.O. Box 9506, 2300 RA Leiden, The Netherlands

<sup>2</sup>Huygens-Kamerlingh Onnes Lab, Universiteit Leiden, P. O. Box 9504, 2300 RA Leiden, The Netherlands

## 1 Interface equation for parallels on axisymmetric surfaces

Our equations are taken from [1], where much wider classes of surfaces were treated and the general stability conditions for the Jülicher-Lipowsky [2] free energy was derived. Here we employ the same notation, and treat the case of *parallel interfaces* on axisymmetric surfaces.

An axisymmetric surfaces can always be explicitly parametrized by a pair of functions  $r(t)$ ,  $z(t)$  which specify the radial profile of the surface as a function of the arc-length parameter  $t$ .  $r$  is the radial distance from the symmetry axis and  $z$  is the axial coordinate. Defining  $\psi = \arctan z'/r'$  to be the azimuthal angle between the surface meridian and the horizontal direction, it can be proven that the geodesic curvature of a parallel is equal to

$$\kappa_g = \frac{\cos \psi}{r}, \quad (1)$$

where the sign convention is that  $\kappa_g$  is positive for interface tangent-normals pointing inside an LD domain. Similarly, the squared mean and Gaussian curvatures are simply

$$H^2 = \frac{1}{4} \left( \frac{\sin \psi}{r} + \psi' \right)^2, \quad K = \frac{\sin \psi}{r} \psi', \quad (2)$$

which are both insensitive to the sign of  $\psi$  and thus to surface orientation. These equations give an explicit form to the terms appearing in Eq. (1) of the main paper. The interface for a given geometry is found after fixing the functions  $r$ ,  $z$  and  $\psi$  and solving the interface equation accordingly.

The highlighted regions of Fig. 5d of the main paper have been numerically found precisely in this manner, after feeding Eq. (1) with a profile consisting of two circles joined by a eighth degree polynomial, whose coefficients have been fixed by requiring that the neck joins the caps smoothly up to the fourth derivative (with two joining points, this gives eight conditions that fix completely the polynomial coefficients). The radii and relative distance of the circles have been fixed by comparing the profile with experimental images. We have verified that changing the polynomial order does not affect our results significantly, indirectly proving that the actual details of the neck are not really relevant for our analysis. This is rather fortunate for our case, since given the small size of the colloids and the resolution of our imaging techniques we cannot resolve the membrane shape much better than Fig. 5a.

If instead the surface is a catenoid, then the equation can be solved analytically. Implicitly, a catenoid is defined by the relation  $r = r_0 \cosh z/r_0$ , with  $r_0$  the minimal neck radius. However, for our case is more convenient to express it in arc-length parametrization as

$$r(t) = \sqrt{r_0^2 + t^2}, \quad z(t) = \frac{r_0}{2} \log \frac{r(t) + t}{r(t) - t}, \quad (3)$$

so that the interface equation becomes

$$t + \frac{\Delta \bar{k}}{\sigma} \frac{r_0^3}{r_0^2 + t^2} = 0, \quad (4)$$

whose solution is the (only) real root of a third order polynomial, namely

$$t = r_0 \left( \frac{D^{1/3}}{2^{1/3}} - \frac{1}{3} \frac{2^{1/3}}{D^{1/3}} \right), \quad \text{with } D = -\frac{\Delta \bar{k}}{\sigma} + \sqrt{\frac{4}{27} + \frac{\Delta \bar{k}^2}{\sigma^2}} > 0. \quad (5)$$

This solution has been used to construct the catenoidal solutions displayed in Fig. 6c.

Similarly, the cone profile is given by the simple linear relation  $r = c|z|$ , which is a well-defined smooth function away from the origin. In fact, in constructing the profile, we take only truncated cones which are cut on the outside by the spherical cup and cut at the vertex by a small parabola connecting the two branches of the cone. The size of this parabolic junction is small with respect to any other scale of the system and ultimately is linked to the resolution of the lithographic printer. The interface equation is even simpler in this case:

$$|z| = \frac{\Delta k}{\sigma} \frac{1}{c^2 \sqrt{1+c^2}}. \quad (6)$$

The values of  $z$  (and of  $r$ ) found from this equation with  $c = 0.75$  have been used to draw the profiles and the interfaces of Figs. 6a-c.

## 2 Supplementary figures

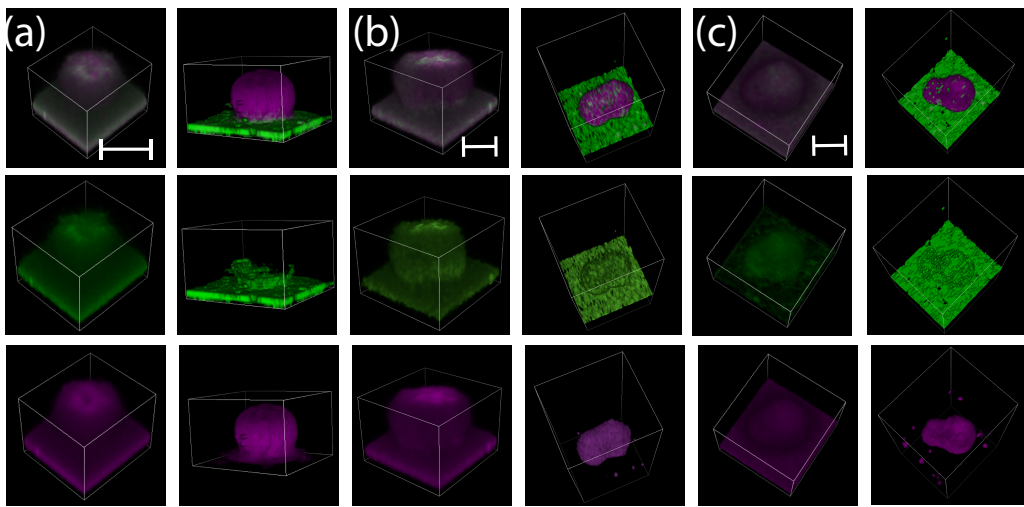


Figure 1: **Single channels images of mixed and phase-separated bilayer on (a) spheres, (b) symmetric, and (c) asymmetric dumbbells of Figure 2 in the main text.** From top to bottom, the overlap image, the green channel and the magenta channel are reported, respectively. Scale bars are  $2 \mu\text{m}$ . The lipid compositions are: BSM:POPC:Chol= 40:50:10 (mixed sphere), 60:20:20 (phase-separated sphere), 20:60:20 (mixed symmetric and asymmetric dumbbells), 20:40:40 (phase-separated symmetric and asymmetric dumbbells).

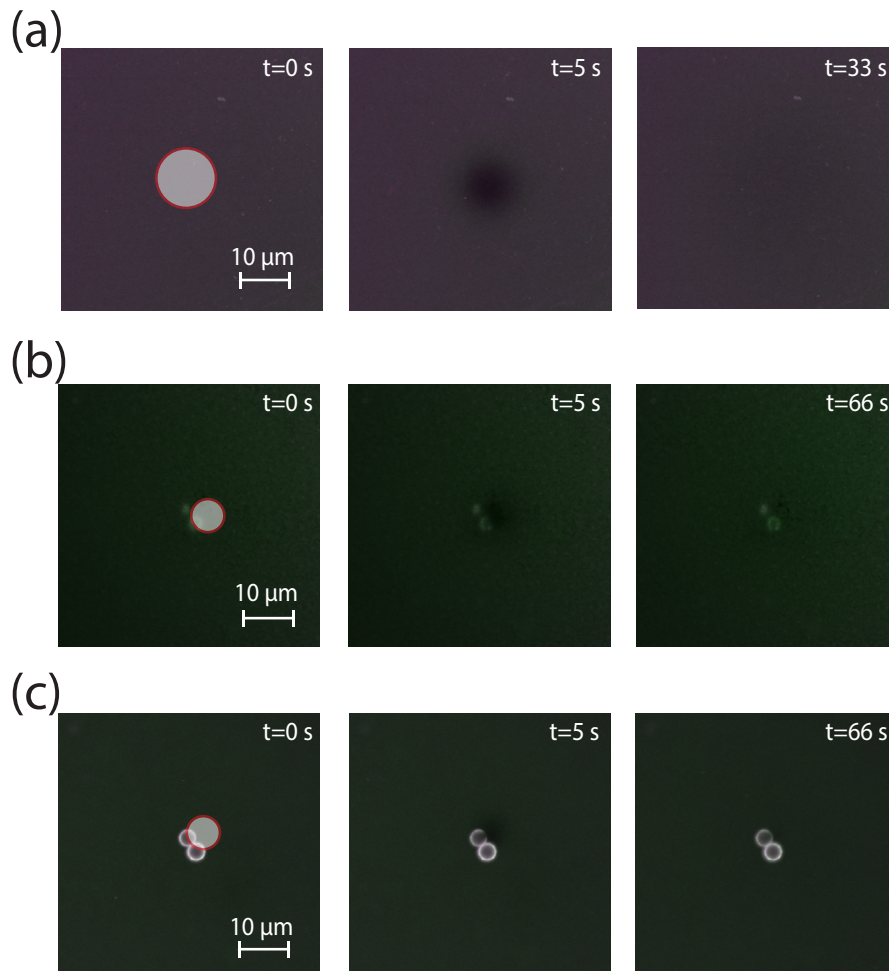


Figure 2: **Fluorescence recovery after photo-bleaching (FRAP) experiment of bilayers on a flat glass substrate (a), in the contact area between substrate and colloid (b), and on a colloid (c).** From left to right: image sequences before bleaching, after bleaching and at the end of the experiment when the signal was recovered. The bleaching areas are indicated in red. The laser used for the bleaching experiment had wavelength 561 nm, also used to image the Rhodamine dye, shown in magenta elsewhere. The lipid compositions are: BSM:POPC:Chol= 20:40:40.

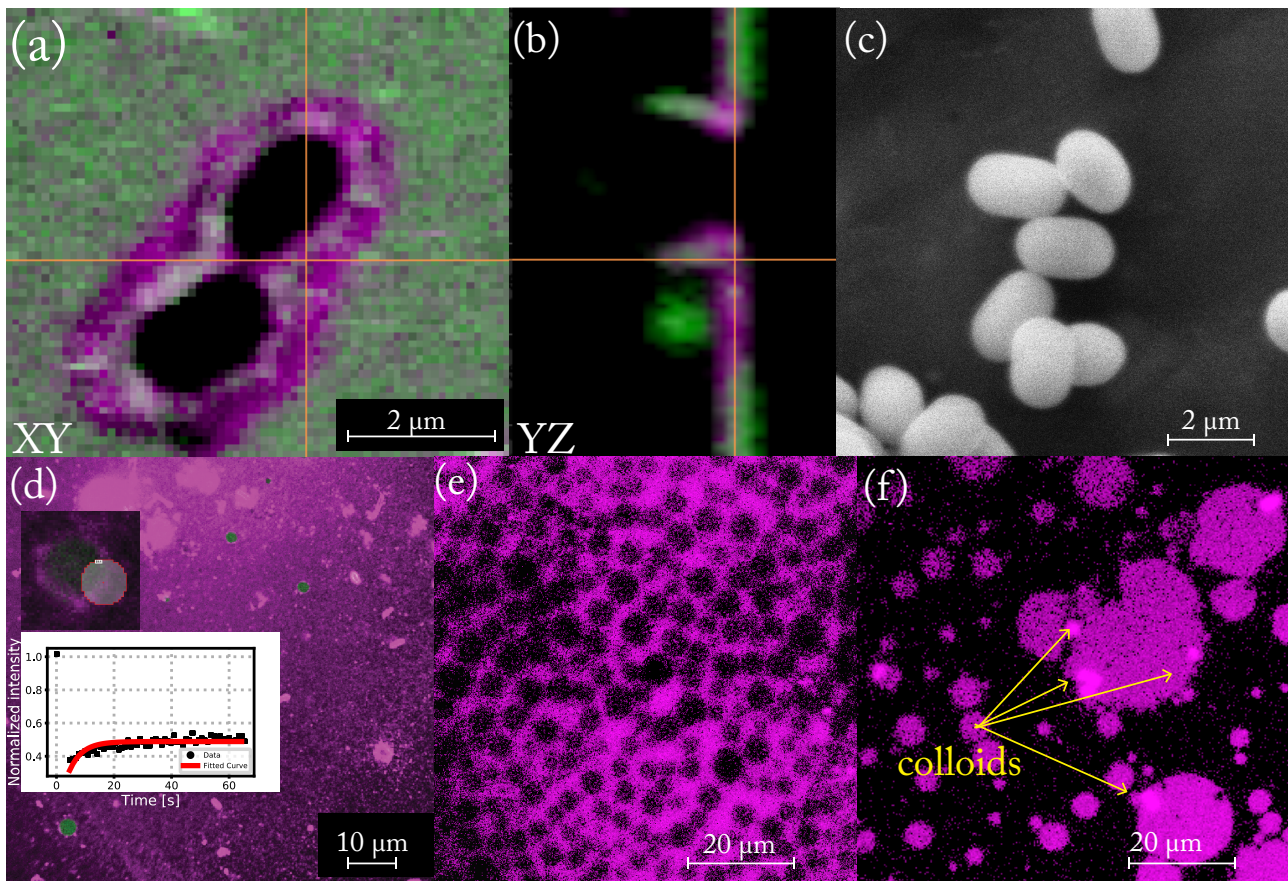


Figure 3: **Phase separation on a flat substrate (a)-(c) Example of a rare case of pinning of the soft phase at the edge between the colloid and the substrate.** This pinning has been observed with a sphero-cylindrical colloid. Fluorescence microscopy image of a lipid bilayer on a cluster of two colloidal sphero-cylinders silica shells obtained from a synthesis procedure analogue to the one of the colloidal cubic shells. The projections of the bilayer on the **(a) XY** and **(b) YZ** planes are reported to show the localisation of the soft phase at the contact area between the colloids and the flat substrate. **(c) SEM** image of the sphero-cylinders. **(d) Fluorescence microscopy image of a lipid bilayer on a flat substrate without colloids taken five days after lipid coating.** Circular LO domains are surrounded by LD domains. In the inset, we report the result of a FRAP experiment on the the bleached area indicated with a red circle. We can observe that the fraction of mobile lipids decreased over the five days. **(e) Fluorescence** image of a phase-separated bilayer on MICA substrate, where only the LD phase was labelled in magenta. We can observe circular domains. **(f) Fluorescence** image of a phase-separated bilayer on a MICA substrate with colloidal particles attached. The particles are indicated in yellow. By comparing the two figures, we can hypothesise that the colloids may alter the regular pattern of circular domains shown in Figure (e). The lipid composition used in all these experiments is BSM:POPC:Chol=50:25:25.

## References

- (1) Fonda, P.; Rinaldin, M.; Kraft, D. J.; Giomi, L. Thermodynamic equilibrium of binary mixtures on curved surfaces. *Physical Review E* **2019**, 100 (3), 032604.
- (2) Jülicher, F.; Lipowsky, R. Domain-induced budding of vesicles. *Physical Review Letters* **1993**, 70 (19), 2964–2967.